



Paleo-ENSO influence on African environments and early modern humans

Stefanie Kaboth-Bahr^{a,b,1}, William D. Gosling^c, Ralf Vogelsang^d, André Bahr^b, Eleanor M. L. Scerri^{d,e,f}, Asfawossen Asrat^{g,h}, Andrew S. Cohenⁱ, Walter Düsing^a, Verena Foerster^j, Henry F. Lamb^{k,l}, Mark A. Maslin^{m,n}, Helen M. Roberts^k, Frank Schäbitz^j, and Martin H. Trauth^a

^aInstitute of Geosciences, University of Potsdam, 14469 Potsdam, Germany; ^bInstitute of Earth Sciences, Heidelberg University, 69120 Heidelberg, Germany; ^cInstitute for Biodiversity and Ecosystem Dynamics, University of Amsterdam, 1098 XE Amsterdam, The Netherlands; ^dDepartment of Prehistoric Archaeology, University of Cologne, 50931 Cologne, Germany; ^ePan-African Evolution Research Group, Max Planck Institute for the Science in Human History, 07745 Jena, Germany; ^fDepartment of Classics and Archaeology, University of Malta, MSD2080, Msida, Malta; ^gSchool of Earth Sciences, Addis Ababa University, 2QM7+CF Addis Ababa, Ethiopia; ^hDepartment of Mining and Geological Engineering, Botswana International University of Science and Technology, Private Bag 16, Palapye, Botswana; ⁱDepartment of Geosciences, University of Arizona, Tucson, AZ 85721; ^jInstitute of Geography Education, University of Cologne, 50931 Cologne, Germany; ^kDepartment of Geography and Earth Sciences, Aberystwyth University, Aberystwyth SY23 3DB, United Kingdom; ^lDepartment of Botany, Trinity College Dublin, Dublin D02 PN40, Ireland; ^mDepartment of Geography, University College London, London WC1E 6BT, United Kingdom; and ⁿNatural History Museum of Denmark, University of Copenhagen, 1165 Copenhagen, Denmark

Edited by J. Tyler Faith, University of Utah, Salt Lake City, UT, and accepted by Editorial Board Member James F. O'Connell April 14, 2021 (received for review September 3, 2020)

In this study, we synthesize terrestrial and marine proxy records, spanning the past 620 ky, to decipher pan-African climate variability and its drivers and potential linkages to hominin evolution. We find a tight correlation between moisture availability across Africa to El Niño Southern Ocean oscillation (ENSO) variability, a manifestation of the Walker Circulation, that was most likely driven by changes in Earth's eccentricity. Our results demonstrate that low-latitude insolation was a prominent driver of pan-African climate change during the Middle to Late Pleistocene. We argue that these low-latitude climate processes governed the dispersion and evolution of vegetation as well as mammals in eastern and western Africa by increasing resource-rich and stable ecotonal settings thought to have been important to early modern humans.

African paleoclimate | hominin evolution | Walker and Hadley circulation | orbital forcing

The role of climatically driven environmental change in triggering key stages of hominin evolution over the last 6 My has long been recognized (1–3). More recently, environmental changes across Africa have been implicated in major shifts in the population structure of hominins over the last half of a million years—the key demographic context for the emergence of *Homo sapiens* (4–8). However, evaluating the impact of environmental changes and their possible effects on hominin evolution and demography is difficult, as high-resolution climate archives are temporally and spatially sparse (9–11). Further problems are introduced by the fact that available proxy studies usually detail climate variability of only one study site or region (3, 12, 13), which makes it difficult to study its consequences for evolutionary processes across large spatial scales. Here, we provide a pan-African view on climate change during the Middle to Late Pleistocene in order to construct a framework for understanding hominin evolution within this timeframe. To achieve this, we have combined 11 terrestrial lacustrine and marine sedimentary archives (Fig. 1 and *SI Appendix, Tables S1 and S2*; see details on site selection criteria in the *SI Appendix*) detailing wet–dry variability of eastern and western Africa during the last 620 ky—the time interval of the emergence of *H. sapiens* in Africa and its subsequent out-of-Africa dispersal (Fig. 1 and *SI Appendix, Table S1*).

Today, the climate of tropical Africa is governed by convection, with the seasonal migration of the tropical rain belt dictating the pattern of precipitation (9). Changes in seasonal positioning of the rain belt relate to insolation variability, with rainfall occurring in northern/southern Africa during boreal/austral summer (14). In addition, observational data suggest that the African climate is highly sensitive to changes in the Walker circulation (WC), which

is manifested via the El Niño Southern Oscillation (ENSO) (15, 16; see *SI Appendix* for more details). ENSO originates from sea surface temperature (SST) anomalies in the equatorial Pacific Ocean, and these changes impact the atmospheric WC, which in turn alters the location and strength of tropical convection cells (Fig. 1) (17). Through this coupled ocean–atmosphere system, ENSO events are propagated around the globe by Kelvin and Rossby waves (16), eventually reaching the African continent (see *SI Appendix* for more details). Here, changes in ENSO state alter the east–west trending moisture gradient across Africa (18–20). This leads to opposing dry and humid conditions between eastern and western Africa so that, during La Niña, eastern Africa experiences drier conditions than western Africa and vice versa during El Niño events. For instance, during El Niño years, eastern Africa experiences positive precipitation anomalies of up to 60% (or 200 mm per year) relative to the yearly precipitation budget during non–El Niño years, while western Africa experiences a 20 to 40% precipitation reduction (21, 22). Besides these modern driving mechanisms, spatiotemporal precipitation changes in Africa on much longer time scales have also been attributed to changes in Atlantic meridional overturning circulation, global atmospheric CO₂ concentrations (*p*CO₂), and/or the waning and waxing of global ice sheets (23–26).

Significance

Our results identify the prime driver of climate variation in Africa's low latitudes over the past 620 ky—the key time frame for the evolution of our species. Warming and cooling of the tropical Pacific Ocean paced by insolation changes modulated the tropical Walker circulation, driving opposing wet–dry states in eastern and western Africa. We show that the effects of glacial/interglacial cycles were not the predominant source of environmental change in most of the continent. Africa's environmental patchwork driven by low-latitude climate processes should therefore be a critical component in conceptual models of human evolution and early demography over the past 620 ky.

Author contributions: S.K.-B. designed research; S.K.-B. analyzed data; and S.K.-B., W.D.G., R.V., A.B., E.M.L.S., A.A., A.S.C., W.D., V.F., H.F.L., M.A.M., H.M.R., F.S., and M.H.T. wrote the paper.

The authors declare no competing interest.

This article is a PNAS Direct Submission. J.T.F. is a guest editor invited by the Editorial Board.

Published under the PNAS license.

¹To whom correspondence may be addressed. Email: kabothbahr@uni-potsdam.de.

This article contains supporting information online at <https://www.pnas.org/lookup/suppl/doi:10.1073/pnas.2018277118/-DCSupplemental>.

Published May 31, 2021.

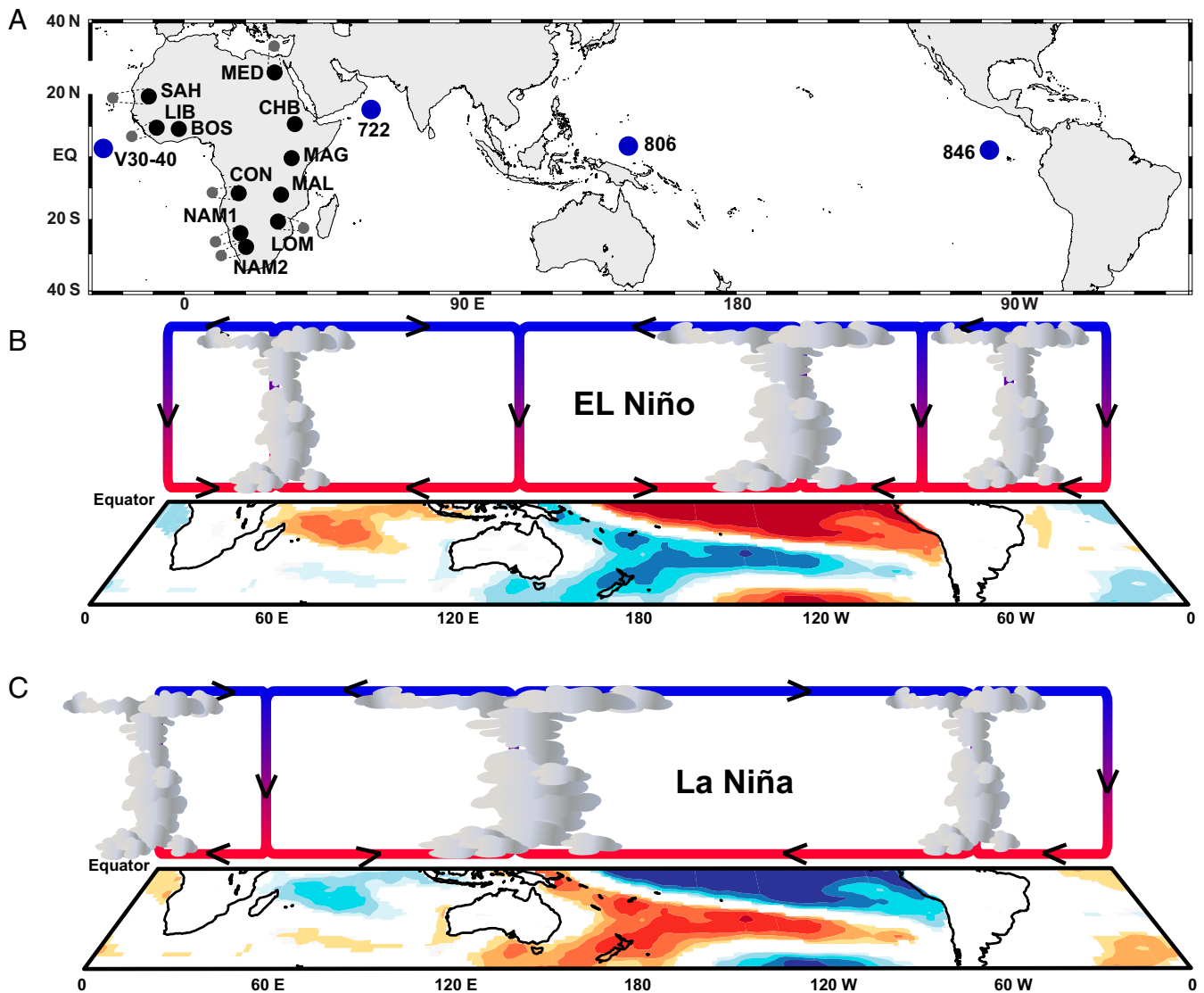


Fig. 1. Suite of study sites and the global WC. (A) Location map of marine and terrestrial proxy records used for the reconstruction of African climate. Note that the black dots associated with marine sites (small gray dots) are referred to their respective hinterland region. SAH = Ocean Drilling Program (ODP) Site 659; LIB = ODP663; BOS = Lake Bosumtwi; CON = ODP Site 1075; NAM1 = GeoB1028-5; NAM2 = ODP Site 1082; LOM = MD96-2048; MAL = Lake Malawi; MAG = Lake Magadi; CHB = Paleolake Chew Bahir; and MED = ODP Site 967. The full list of references and coordinates for all sites is provided in *SI Appendix, Table S1*. Blue dots mark marine sites used for the reconstruction of the WC (*SI Appendix, Table S2*). (B) SST anomalies and resulting changes in tropical heating and convection (related to WC) under El Niño conditions (positive ENSO phase). (C) SST anomalies and resulting changes in tropical heating and convection (related to WC) under La Niña conditions (negative ENSO phase). For more details on the effect of El Niño/La Niña on African precipitation, see *SI Appendix*. Blue areas = cooling relative to normal conditions; red areas = warming relative to normal conditions; and black arrows indicate transport direction.

However, the interplay of these various driving mechanisms on orbital time scales and their pan-African impact on precipitation remains ambiguous.

Results

Our study elucidates the spatiotemporal variability of the African hydroclimate and its driving forces by providing a comprehensive analysis of pan-African climate change during the last ~620 ky. To parametrize pan-African climate variability, we performed a piecewise principal component analysis (pwPCA; see *Materials and Methods* for details) of the selected datasets (see Figs. 1 and 2) to account for differences in temporal length of the records. The resulting first principal component (PC1), capturing the maximum variance of the data, accounts on average for 30% of the variance observed in all the datasets and clearly depicts an east–west dipole of the studied sites (Fig. 2B). Remaining principal components

(PCs) account individually for less than 10% of the remaining data variance. This suggests that the observed east–west dipole is the predominant mode of signal variability on a pan-African scale during the last ~620 ky. In detail, the eastern African sites (CHB, MED, MAG, and LOM, reflecting the negative PC1 branch; Fig. 1) oppose western African sites (SAH, BOS, LIB, CON, NAM1, and NAM2, reflecting the positive PC1 branch; Fig. 1). MAL located in southeastern Africa is weakly in phase with the western African sites. Note here that the applied age model for MAL is one of several possibilities. Please see *SI Appendix* for the PC1 comparison based on different MAL age models.

The reconstructed pan-African climate variability, represented by PC1, clearly depicts four phases during the last ~620 ky that have been constrained by breakpoint analysis (Fig. 2C; see *Materials and Methods* for details). Phase I lasts from ~620 to ~525 ky and is characterized by more humid conditions in eastern

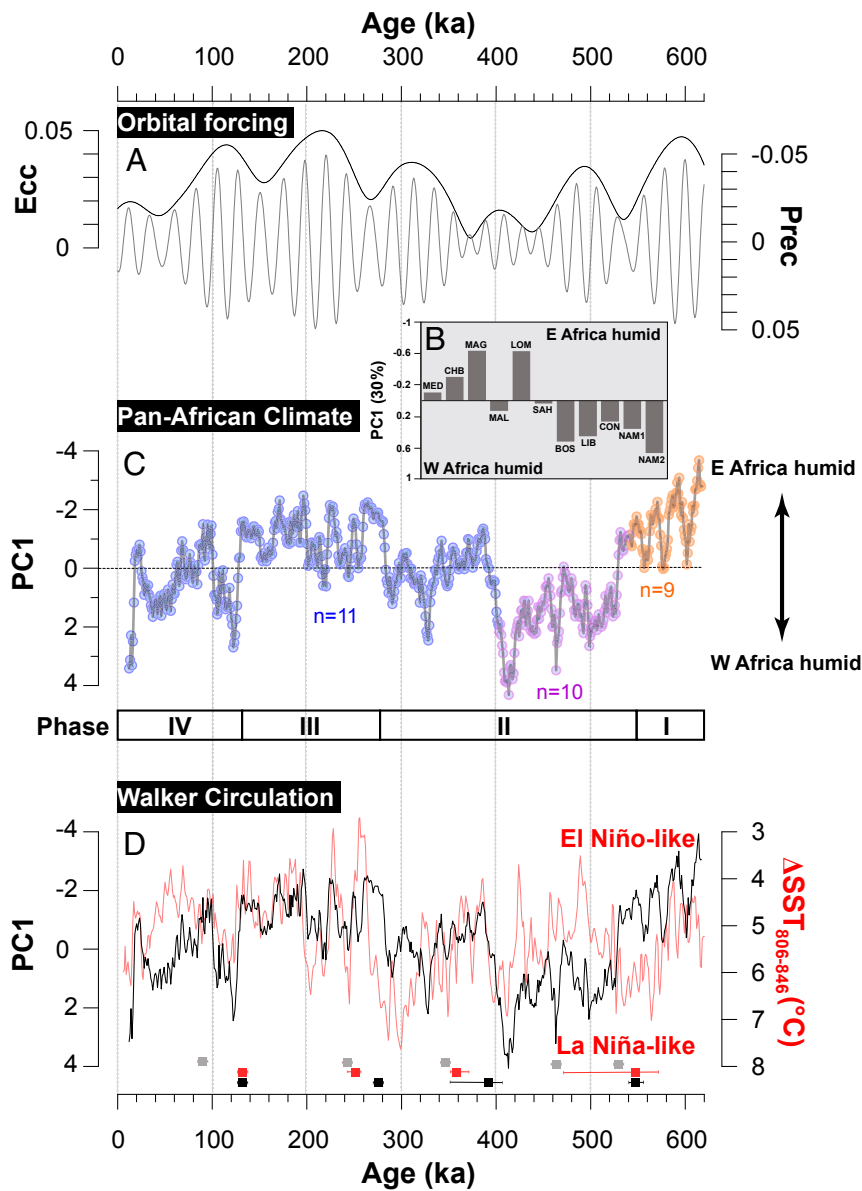


Fig. 2. Pan-African climate variability during the last ~620 ky. (A) Orbital eccentricity (Left) and precession (Right) (59). (B) Average PC1 loadings derived from the pwPCA. (C) PC1 derived from the pwPCA. n = number of datasets used in each iteration. (D) Comparison between PC1 and the SST gradient (Δ SST; red line) between eastern Pacific Ocean Drilling Program (ODP) Site 806 (32) and western Pacific Ocean ODP Site 846 (33). Designation of El Niño- and La Niña-like conditions follows ref. 30. Breakpoints and their error bounds of PC1 (black boxes), ENSO (red boxes), and Earth's eccentricity (gray boxes) are marked.

Africa and more arid conditions in western Africa (i.e., PC1 shows more negative values). This pattern reverses during the subsequent Phase II between ~525 and ~279 ky, when above average humid conditions prevail in western Africa, while eastern Africa experiences more arid conditions (i.e., PC1 shows more positive values). Notably, Phase II encompasses two subphases with a transition at around ~400 ky. However, the median over the entire variability of Phase II is significantly more positive in its PCA loadings than Phases I and III. Based on this difference, we decided to group both subphases into Phase II. During Phase III, between ~279 and ~128 ky, this relationship once again reverses with pronounced humid conditions prevailing in eastern Africa and arid conditions in western Africa. Late Phase III aligns, within the limitation of the age uncertainties, with the well-documented wet phase associated with the last interglacial (~129 to 119 ky) (12). During the last

~128 ky (Phase IV), more humid conditions prevailed in western Africa, in contrast to a drier eastern Africa.

Discussion

In order to decipher the mechanism behind the observed pan-African moisture pattern, we first considered low-latitude insolation changes as a strong contributor, given the well-documented sensitivity of tropical climate to insolation changes (27). Thus, we first compared the PC1 to precession and orbital eccentricity variability for the studied time interval (Fig. 2A). PC1 clearly follows the distinctive ~400 and ~100 ky beats of eccentricity, which is further supported by the near synchronicity of the breakpoints calculated from PC1 and orbital eccentricity forcing (Fig. 2). This coherent pattern suggests that on geological time scales, precipitation changes in tropical Africa are in large part paced by insolation changes (28). However, by itself, eccentricity only has a small

net effect on the annual mean insolation (<0.5%). Instead, it exerts a strong pull on the amplitude change of orbital precession (29). The difference in precession amplitude can amount to ~10% of the annual mean insolation (20). Changes in the annual insolation budget, and thus increased/decreased regional convection above the African continent, could potentially explain the difference between northern and southern Africa, as it does today on seasonal time-scales. However, it does not fully explain the east–west moisture dipole apparent in PC1. To explain this conundrum, we thus require an insolation-sensitive mechanism that generates zonal changes in precipitation. We hypothesize that ENSO-like variability might be the key to unravel this enigma. It has been demonstrated that ENSO modulated Earth's climate during the geological past (28, 29). Also, it has been shown that ENSO variability is sensitive to insolation changes (17), with high/low eccentricity (increased/decreased insolation) aligning with El Niño/La Niña-like conditions (30). Finally, modern ENSO-related modifications in the WC (31) result in a westward/eastward shift of convection over Africa (15, 18).

To ground truth the potential role of ENSO-like fluctuations for generating the observed zonal precipitation gradients, we compared PC1 to the east–west SST gradient of the Pacific Ocean ($\Delta\text{SST}_{806-846}$; Fig. 2D) during the last ~620 ky (32, 33). A strong positive ΔSST indicates a warmer west Pacific relative to a colder east Pacific Ocean, similar to modern La Niña conditions. On the other hand, a strongly reduced $\Delta\text{SST}_{806-846}$ suggests a warming in the east Pacific Ocean and thus resembles modern El Niño conditions (30). The comparison shows a strong resemblance between PC1 and $\Delta\text{SST}_{806-846}$ throughout the last ~620 ky, which is further supported by similar timed breakpoints in both records (Fig. 2). This implies that the dominant climate signal follows a paleo-ENSO beat, with contrasting effects in eastern and western Africa. This suggests that traces of the hypothesized WC shifts induced by ENSO variability during the last ~620 ky should also be preserved in proxy records from the Atlantic and Indian Ocean. Indeed, the analysis of the SST variability of Arabian Sea Ocean Drilling Program (ODP) Site 722 clearly depicts a strong warming during the proposed El Niño-like condition of Phase III (33), in line with our expectation (SI Appendix, Fig. S2). The simultaneous formation of the Atlantic cold tongue, as previously proposed, is also visible in the SST cooling during Phase III of tropical Atlantic Ocean site V30-40 (34). This provides further strong indication of the sensitivity of the pan-African moisture budget to changes in the WC during the last ~620 ky (SI Appendix, Fig. S2).

The results we present here provide a framework for understanding East–West contrasts in Africa's climatic history on geological time scales, which has important implications for testing hypotheses regarding human evolution and the dispersal of early modern humans. For this, we have outlined the spatiotemporal effects of ENSO-like variability during Phases II to IV, comprising a full ~400 ky eccentricity cycle in Fig. 3. We find that during eccentricity minima and ensuing La Niña-like conditions (i.e., Phases II and IV) regions of low topographic complexity (35) from the Sahel to Namibia were preconditioned to wetter conditions (Fig. 3D and F). In contrast, eccentricity maxima, and thus El Niño-like conditions (i.e., Phase III), favored a moisture increase across the topographically more complex and geographically smaller eastern Africa (Fig. 3E) (35). Although our analysis does not allow for the quantification of the observed relative humidity changes, these paleoclimatic changes and their effects on terrestrial ecosystems are likely to have impacted human dispersal and evolution. While the association between climate and the human record is typically neither simple nor direct, key linkages can be identified through proxy archives of vegetation changes, as well as the mammalian record (36). In fact, our inferred paleo-ENSO-driven humidity changes coincide with major changes in vegetation across the African continent during the last ~500 ky. At the available terrestrial, landscape scale (i.e., tens of kilometers), pollen-based reconstructions of past vegetation change at Lake Bosumtwi (western Africa) during the last

~540 ky indicate oscillations between open forest and wooded savanna during La Niña-like conditions (Phase IV and II) and treeless savanna coinciding with El Niño-like conditions (Phase III) (37). The reverse is true for Lake Magadi (eastern Africa), where abundant Afromontane and woodland elements dominate during the El Niño phase (Phase III) and the expansion of the savanna during the La Niña phases (Phase II and IV) (3). Additionally, marine pollen records, which integrate a vegetation signal from a wide geographic area (i.e., hundreds of kilometers), suggest a major perturbation on a pan-African scale at around ~128 ky (38).

The impact of the inferred paleo-ENSO-induced reorganization of the African climate system and associated changes in vegetation likely also had a profound ecological impact on mammal species across Africa. While the genetic diversity of many mammals is known to strongly reflect ecoregion biogeographic history and fragmentation, the driving factors for these community-wide patterns of vicariance are usually assumed to relate to environmental changes driven by climatic variability (39, 40). Interestingly, basal divisions during the Middle to Late Pleistocene between taxa repeatedly followed an oblique divide between western–central African populations and eastern–southern African populations that corresponds well with the rainfall dipole in our conceptual model (39–43). In addition, several studies attempting to constrain the timing of divergence in African mammals suggest that splits are out of phase with glacial–interglacial cycles and instead linked population isolation and habitat fragmentation with pronounced, insolation-driven oscillations between wet and dry conditions (41, 42). These time estimates for divergence correspond well with our proposed climatic phases. For example, the transition between Phase II and III, which saw the shift from wet to arid conditions in western–central Africa, dovetails with a general radiation of giraffe (*Cervus camelopardalis*), lion (*Panthera leo*), and hartebeest (*Alcelaphus buselaphus*), particularly with estimated split times between west/north and east/south clades (41, 42, 44). Additionally, the transition from Phase III to IV, which featured the return of wet/dry conditions in western–central/eastern–southern Africa, corresponds with successive branching and population increase among giraffe, lion, and hartebeest in both regions (41, 42, 44). Many other taxa exhibit similar patterns, including African buffalo (*Syncerus caffer*), roan (*Hippotragus equinus*), waterbuck (*Kobus ellipsiprymnus*), kob (*Kobus kob*), warthog (*Phacochoerus africanus*), topi (*Damaliscus lunatus jimela*), and bushbuck (*Tragelaphus scriptus*) (40, 41, 43, 45). Specifically, phylogenetic patterns indicate the presence of refugial zones for savannah and grassland species in western Africa, southern Africa, and a refugial mosaic/suture zone in eastern Africa. These areas likely played a key role in fragmenting savannah and grassland species during the alternating periods of forest expansion associated with wetter conditions in western–central Africa or eastern Africa (42, 43, 46–48).

Although no ancient African DNA from these time frames is available for humans, it seems likely that hominin populations have followed a similar pattern. Our findings are in fact consistent with previous studies that have indicated that archaeological site abundances in eastern Africa and elsewhere in tropical Africa are both inversely related up to 60 ka and do not strongly align with glacial–interglacial cycles (49). Increases in abundance seem to correlate with periods of decreased humidity (e.g., between ~115 to 90 ka in tropical Africa), while decreases seem to correlate with increased humidity (e.g., between ~110 to 95 ka in eastern Africa), both of which fall within our Phase IV (49). The effects of the reconstructed paleo-ENSO variability likely caused forest fragmentation in eastern and western Africa during dry phases, which would have increased the size of ecotonal regions, that have long been argued to represent resource rich and, therefore, preferred habitats for hominins (49–51). Ecotonal areas may have provided important zones of habitat stability and population growth during the identified phases (Fig. 3) and, critically, are also linked to the success of other African generalist mammals (40). These spatial

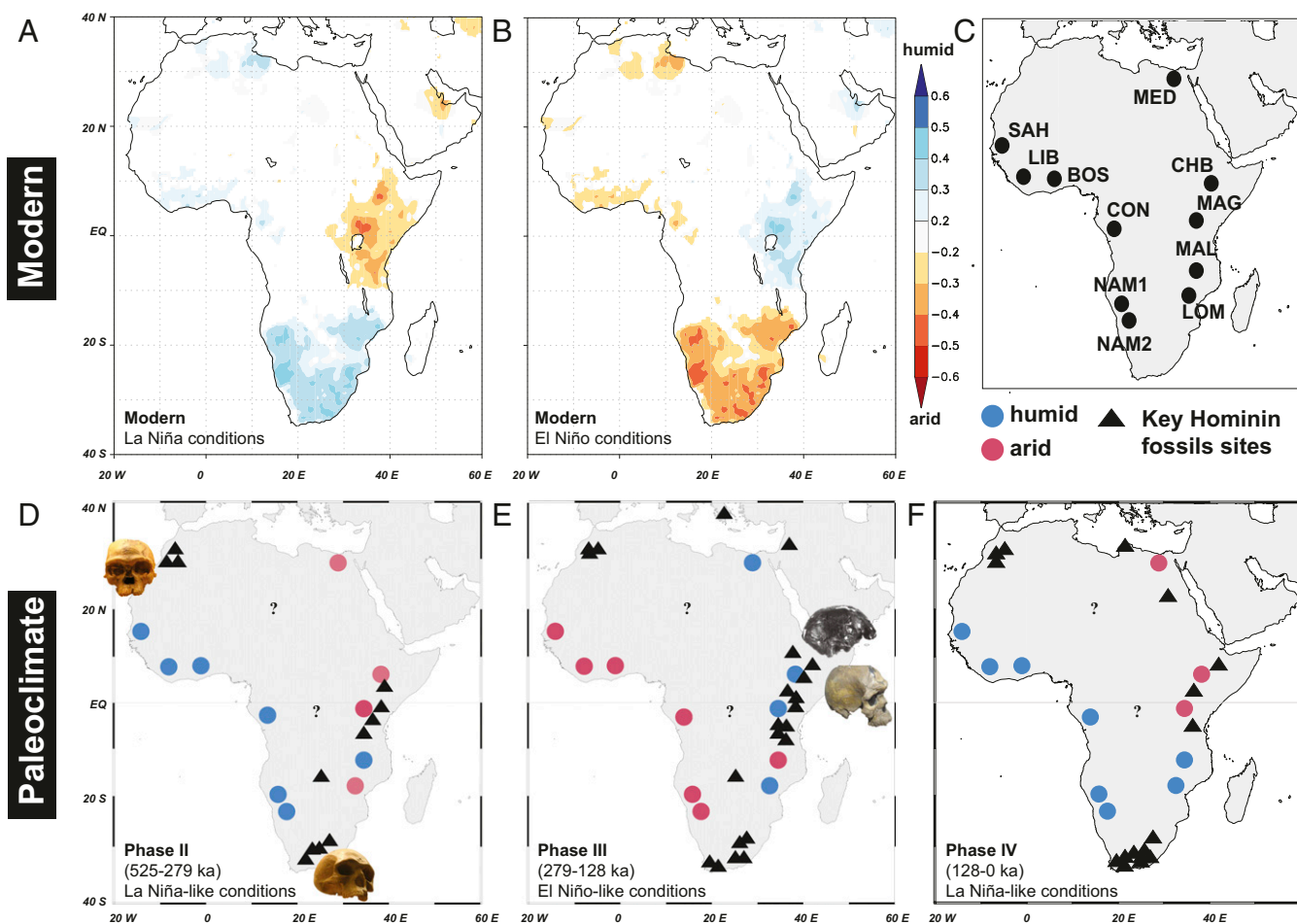


Fig. 3. Pan-African climate variability relative to the fossil evidence for hominin evolution during the Middle and Late Pleistocene. *A* and *B* show the Spearman correlation coefficients for the months October to April from years 1891 to 2016 of the NINO3.4 index and the Global Precipitation Climatology Centre (V2018 land) precipitation data in a 0.5° grid. Positive correlation coefficients = humid conditions; negative correlation coefficients = arid conditions. The spatial correlation shown is significant with $P > 10\%$. Analysis and visualization can be found at the following: <https://climexp.knmi.nl/start.cgi>. *C* displays the location of the study sites used for the reconstruction of pan-African climate variability. The full list of abbreviations, references, and coordinates for all sites is provided in *SI Appendix, Table S1*. *D–F* present the spatiotemporal distribution of moisture during Phases II, III, and IV, thus encompassing a full ~400-ky eccentricity cycle. The designation of humid/arid (blue/red) for each study site (circle) derives from the calculation of the proxy median for the respective time slice relative to the reference median value of the entire data population across the last ~620 ky (see *Materials and Methods* for details; *SI Appendix, Table S3*). The list of key hominin fossil sites traces are marked by black triangles (see *SI Appendix, Table S4* for references). Photographs in *D* are from Ryan Somma/Wikimedia Commons. Photographs in *E* from the top, modified from ref. 60, are from Addis Ababa National Museum/Wikimedia Commons.

patterns may explain past population structures, reflecting deep regional subdivisions that are likely to have been even more pronounced in the Middle and Late Pleistocene (7, 8, 48, 52–54).

Conclusion

Our results highlight a tight correlation between moisture availability in Africa and WC changes, most likely induced by paleo-ENSO variability. This process causes a distinct east–west dipole, with humid condition on one side of Africa and arid conditions on the other. We argue that the pacing of this low-latitude process governed the dispersion and evolution of vegetation, as well as mammals, in eastern and western Africa and likely also drove shifts in the degree of structure, population density, and core habitation areas of hominins. These results, therefore, provide a framework to test a range of conceptual models regarding the multiregional rise and subsequent dispersal of hominins (8), in which glacial–interglacial cyclicity can no longer be uncritically invoked as the predominant climatic driver.

Materials and Methods

pwPCA. PCA detects linear dependencies between variables and replaces groups of linear correlated variables with new, uncorrelated variables referred to as the PCs. Since the PC1 contains the highest variance and the PC2 the second highest variance, the last PCs are ignored to reduce the dimensions of the data. The principal component loadings (i.e., the coefficients of the linear combination of the initial variables from which the principal components are constructed) can be used to interpret the PCs and hence to identify (or display) dominant variability patterns in time series. Prior to the application of the pwPCA, all datasets were resampled at 1 ky resolution. All data were standardized to unit variance using their individual mean and SD. Prior to standardization, we also log transformed the datasets of CHB, LOM, SAH, BOS, LIB, CON, NAM1, and NAM2 (see *SI Appendix, Table S1* for acronyms) to account for outlier-induced data skewing and thus more closely approximate a normal distribution for these datasets. For the pwPCA, the entire dataset was separated into three timeframes, fitting to the individual shortest dataset of each timeframe (Fig. 2). This leads to a decrease of datasets and thus an increase of uncertainties with increasing time. PCA was conducted using the built-in function *princomp* in R (55). Loadings and explained variance of the PC1 was averaged over all time steps of the pwPCA.

Breakpoint Analysis. The breakpoints derive from a fitting of a linear regression model to the dataset, as implemented in the *strucchange* package in R (56). The algorithm tests deviations from stability in a classical linear regression model, with a preset of maximum $m = 5$ breakpoints. The integrated optimization algorithm provides the optimized location of the breakpoints, as well as their 2.5 and 97.5% confidence intervals.

Median Calculation. To analyze long-term changes in the moisture of each individual site, we calculated the median over the full length of the respective dataset as a cutoff value between humid and arid conditions. Subsequently, we calculated the median for Phase II to IV only, following the age designation of PC1 as stated in the main text, and compared it to the overall cutoff value. Following the individual interpretation of the proxy records (*SI Appendix, Table S1*), we assigned each phase to overall humid or arid conditions. For MED and BOS cutoff, values of 0 and 57 were already defined in the respective publication (57, 58).

Data Availability. All study data are included in the article and/or supporting information.

ACKNOWLEDGMENTS. S.K.-B. received funding from an Open Topic Postdoctoral fellowship from the University of Potsdam and acknowledges funding from the Deutsche Forschungsgemeinschaft (DFG) through Grant KA 4757/3-1. Support for Chew Bahir drilling was provided by DFG through the Priority Program SPP 1006 International Continental Drilling Program, as well as through NSF Grant NSF-EAR1338553 to A.S.C. F.S. acknowledges further funding from the DFG through Grants SCHA 472/13 and SCHA 472/18. M.H.T. acknowledges funding from the DFG through Grants TR 419/8, TR 419/10, and TR 419/16. In addition, F.S. acknowledges funding from the Collaborative Research Centre 806 Research Project “Our way to Europe”—Project Number 57444011. H.F.L. and H.M.R. were funded by Grant NE/K014560/1 from the UK Natural Environment Research Council. This is publication No. 36 of the Hominin Sites and Paleolakes Drilling Project. All data used in the analysis are available through their respective references. The results of the pwPCA is appended as supporting information.

1. J. Galway-Witham, J. Cole, C. Stringer, Aspects of human physical and behavioural evolution during the last 1 million years. *J. Quat. Sci.* **34**, 355–378 (2019).
2. N. E. Levin, Environment and climate of early human evolution. *Annu. Rev. Earth Planet. Sci.* **43**, 405–429 (2015).
3. R. B. Owen *et al.*, Progressive aridification in East Africa over the last half million years and implications for human evolution. *Proc. Natl. Acad. Sci. U.S.A.* **115**, 11174–11179 (2018).
4. C. M. Schlebusch *et al.*, Genomic variation in seven Khoe-San groups reveals adaptation and complex African history. *Science* **338**, 374–379 (2012).
5. C. M. Schlebusch *et al.*, Southern African ancient genomes estimate modern human divergence to 350,000 to 260,000 years ago. *Science* **358**, 652–655 (2017).
6. M. Lipson *et al.*, Ancient West African foragers in the context of African population history. *Nature* **577**, 665–670 (2020).
7. E. M. L. Scerri *et al.*, Did our species evolve in subdivided populations across Africa, and why does it matter? *Trends Ecol. Evol.* **33**, 582–594 (2018).
8. E. M. L. Scerri, L. Chikhi, M. G. Thomas, Beyond multiregional and simple out-of-Africa models of human evolution. *Nat. Ecol. Evol.* **3**, 1370–1372 (2019).
9. R. Potts, Evolution and climate variability. *Science* **273**, 922–923 (1996).
10. P. Roberts, B. A. Stewart, Defining the ‘generalist specialist’ niche for Pleistocene *Homo sapiens*. *Nat. Hum. Behav.* **2**, 542–550 (2018).
11. A. Mounier, M. Mirazón Lahr, Deciphering African late middle Pleistocene hominin diversity and the origin of our species. *Nat. Commun.* **10**, 3406 (2019).
12. H. F. Lamb *et al.*, 150,000-year palaeoclimate record from northern Ethiopia supports early, multiple dispersals of modern humans from Africa. *Sci. Rep.* **8**, 1077 (2018). Correction in: *Sci. Rep.* **8**, 17993 (2018).
13. S. J. Ivory *et al.*, Environmental change explains cichlid adaptive radiation at Lake Malawi over the past 1.2 million years. *Proc. Natl. Acad. Sci. U.S.A.* **113**, 11895–11900 (2016).
14. S. E. Nicholson, Climate and climatic variability of rainfall over eastern Africa. *Rev. Geophys.* **55**, 590–635 (2017).
15. S. E. Nicholson, J. C. Selato, The influence of La Nina on African rainfall. *Int. J. Climatol.* **20**, 1761–1776 (2000).
16. F. S. R. Pausata *et al.*, Greening of the Sahara suppressed ENSO activity during the mid-Holocene. *Nat. Commun.* **8**, 16020 (2017).
17. P. J. Webster, “The large-scale structure of the tropical atmosphere” in *General Circulation of the Atmosphere*, J. Hoskins, R. P. Pearce, Eds. (Academic Press, San Diego, CA, 1983), pp. 35–275.
18. C. P. de Oliveira, L. Aimola, T. Ambrizzi, A. C. V. Freitas, The influence of the regional Hadley and Walker circulations on precipitation patterns over Africa in El Niño, La Niña, and neutral years. *Pure Appl. Geophys.* **175**, 2293–2306 (2018).
19. N. H. Saji, B. N. Goswami, P. N. Vinayachandran, T. Yamagata, A dipole mode in the tropical Indian Ocean. *Nature* **401**, 360–363 (1999).
20. D. J. Nash *et al.*, African hydroclimatic variability during the last 2000 years. *Quat. Sci. Rev.* **154**, 1–22 (2016).
21. I. Fer, B. Tietjen, F. Jeltsch, C. Wolff, The influence of El Niño-Southern Oscillation regimes on eastern African vegetation and its future implications under the RCP8.5 warming scenario. *Biogeosciences* **14**, 4355–4374 (2017).
22. S. M. Moore *et al.*, El Niño and the shifting geography of cholera in Africa. *Proc. Natl. Acad. Sci. U.S.A.* **114**, 4436–4441 (2017).
23. J. E. Kutzbach, F. A. Street-Perrott, Milankovitch forcing of fluctuations in the level of tropical lakes from 18 to 0 kyr BP. *Nature* **317**, 130–134 (1985).
24. M. H. Trauth, M. A. Maslin, A. Deino, M. R. Strecker, Late Cenozoic moisture history of east Africa. *Science* **309**, 2051–2053 (2005).
25. I. S. Castañeda *et al.*, Wet phases in the Sahara/Sahel region and human migration patterns in North Africa. *Proc. Natl. Acad. Sci. U.S.A.* **106**, 20159–20163 (2009).
26. P. N. DiNezio *et al.*, Glacial changes in tropical climate amplified by the Indian Ocean. *Sci. Adv.* **4**, eaat9658 (2018).
27. A. C. Clement, R. Seager, M. A. Cane, Orbital controls on the El Niño/Southern Oscillation and the tropical climate. *Paleoceanography* **14**, 441–456 (1999).
28. A. Davies, A. E. S. Kemp, G. P. Weedon, J. A. Barron, El Niño-Southern oscillation variability from the late cretaceous marra shale of California. *Geology* **40**, 15–18 (2012).
29. T. Laepple, G. Lohmann, Seasonal cycle as template for climate variability on astronomical timescales. *Paleoceanography* **24**, PA4201 (2009).
30. Y. G. Zhang, J. Ji, W. L. Balsam, L. Liu, J. Chen, High resolution hematite and goethite records from ODP 1143, South China Sea: Co-evolution of monsoonal precipitation and El Niño over the past 600,000 years. *Earth Planet. Sci. Lett.* **264**, 136–150 (2007).
31. M. L. L’Heureux, S. Lee, B. Lyon, Recent multidecadal strengthening of the Walker circulation across the tropical Pacific. *Nat. Clim. Chang.* **3**, 571–576 (2013).
32. M. Medina-Elizalde, D. W. Lea, The mid-Pleistocene transition in the tropical Pacific. *Science* **310**, 1009–1012 (2005).
33. T. D. Herbert *et al.*, Late Miocene global cooling and the rise of modern ecosystems. *Nat. Geosci.* **9**, 843–847 (2016).
34. A. McIntyre, W. F. Ruddiman, K. Karlin, A. C. Mix, Surface water response of the equatorial Atlantic Ocean to orbital forcing. *Paleoceanography* **4**, 19–55 (1989).
35. G. N. Bailey, G. C. P. King, Dynamic landscapes and human dispersal patterns: Tectonics, coastlines, and the reconstruction of human habitats. *Quat. Sci. Rev.* **30**, 1533–1553 (2011).
36. A. K. Behrensmeier, Atmosphere. Climate change and human evolution. *Science* **311**, 476–478 (2006).
37. C. S. Miller, W. D. Gosling, Quaternary forest associations in lowland tropical West Africa. *Quat. Sci. Rev.* **84**, 7–25 (2014).
38. L. Dupont, Orbital scale vegetation change in Africa. *Quat. Sci. Rev.* **30**, 3589–3602 (2011).
39. M. de Manuel *et al.*, The evolutionary history of extinct and living lions. *Proc. Natl. Acad. Sci. U.S.A.* **117**, 10927–10934 (2020).
40. Y. Moodley, M. W. Bruford, Molecular biogeography: Towards an integrated framework for conserving pan-African biodiversity. *PLoS One* **2**, e454 (2007).
41. D. M. Brown *et al.*, Extensive population genetic structure in the giraffe. *BMC Biol.* **5**, 57 (2007).
42. L. D. Bertola *et al.*, Phylogeographic patterns in Africa and high resolution delineation of genetic clades in the lion (*Panthera leo*). *Sci. Rep.* **6**, 30807 (2016).
43. E. D. Lorenzen, R. Heller, H. R. Siegmund, Comparative phylogeography of African savannah ungulates. *Mol. Ecol.* **21**, 3656–3670 (2012).
44. O. Flagstad, P. O. Syvertsen, N. C. Stenseth, K. S. Jakobsen, Environmental change and rates of evolution: The phylogeographic pattern within the hartebeest complex as related to climatic variation. *Proc. Biol. Sci.* **268**, 667–677 (2001).
45. R. Barnett, N. Yamaguchi, I. Barnes, A. Cooper, The origin, current diversity and future conservation of the modern lion (*Panthera leo*). *Proc. Biol. Sci.* **273**, 2119–2125 (2006).
46. G. Hewitt, The genetic legacy of the Quaternary ice ages. *Nature* **405**, 907–913 (2000).
47. J. T. Faith, J. Rowan, K. O’Brien, N. Blegen, D. J. Peppe, Late Pleistocene mammals from Kibogo, Kenya: Systematic paleontology, paleoenvironments, and non-analog associations. *J. Vertebr. Paleontol.* **40**, e1841781 (2020).
48. J. T. Faith *et al.*, Paleoenvironmental context of the Middle Stone Age record from Karungu, Lake Victoria Basin, Kenya, and its implications for human and faunal dispersals in east Africa. *J. Hum. Evol.* **83**, 28–45 (2015).
49. M. W. Blome, A. S. Cohen, C. A. Tryon, A. S. Brooks, J. Russell, The environmental context for the origins of modern human diversity: A synthesis of regional variability in African climate 150,000–30,000 years ago. *J. Hum. Evol.* **62**, 563–592 (2012).
50. L. S. Basell, Middle Stone Age (MSA) site distributions in eastern Africa and their relationship to Quaternary environmental change, refugia and the evolution of *Homo sapiens*. *Quat. Sci. Rev.* **27**, 2484–2498 (2008).
51. C. Shipton *et al.*, 78,000-year-old record of Middle and Later Stone Age innovation in an East African tropical forest. *Nat. Commun.* **9**, 1832 (2018). Correction in: *Nat. Commun.* **9**, 2242 (2018).
52. A. Bergström *et al.*, Insights into human genetic variation and population history from 929 diverse genomes. *Science* **367**, eaay5012 (2020).
53. E. M. L. Scerri *et al.*, Continuity of the Middle Stone Age into the Holocene. *Sci. Rep.* **11**, 70 (2021).
54. A. Bergström, C. Stringer, M. Hajdinjak, E. M. L. Scerri, P. Skoglund, Origins of modern human ancestry. *Nature* **590**, 229–237 (2021).
55. W. N. Venables, B. D. Ripley, *Modern Applied Statistics with S* (Springer, ed. 4, 2002).
56. A. Zeileis, C. Kleiber, W. Krämer, K. Hornik, Testing and dating of structural changes in practice. *Comput. Stat. Data Anal.* **44**, 109–123 (2003).
57. K. M. Grant *et al.*, A 3 million year index for North African humidity/aridity and the implication of potential pan-African Humid periods. *Quat. Sci. Rev.* **171**, 100–118 (2017).
58. C. S. Miller, W. D. Gosling, D. B. Kemp, A. L. Coe, I. Gilmore, Drivers of ecosystem and climate change in tropical West Africa over the past ~540 000 years. *J. Quat. Sci.* **31**, 671–677 (2016).
59. J. Laskar *et al.*, A long-term numerical solution for the insolation quantities of the Earth. *Astron. Astrophys.* **428**, 261–285 (2004).
60. I. McDougall, F. H. Brown, J. G. Fleagle, Stratigraphic placement and age of modern humans from Kibish, Ethiopia. *Nature* **433**, 733–736 (2005).